Saudi Journal of Biological Sciences (2017) **24**, 1392–1403

King Saud University

Saudi Journal of Biological Sciences

www.ksu.edu.sa
www.sciencedirect.com

ORIGINAL ARTICLE

In-vitro cytotoxicity and cellular uptake studies of luminescent functionalized core-shell nanospheres

Anees A. Ansari [a,*], T.N. Hasan [b], N.A. Syed [b], J.P. Labis [a], Ali A. Alshatwi [b]

[a] *King Abdullah Institute for Nanotechnology, King Saud University, P.O. Box 2455, Riyadh 11451, Saudi Arabia*
[b] *Molecular Cancer Biology Research Lab (MCBRL), Department of Food Science and Nutrition, King Saud University, Riyadh 11451, Saudi Arabia*

Received 14 December 2015; revised 18 April 2016; accepted 30 August 2016
Available online 8 September 2016

KEYWORDS

Core-shell nanospheres;
HepG2 cells;
Toxicity;
Apoptosis;
Bio-labeling

Abstract Monodispersed luminescent functionalized core-shell nanospheres (LFCSNs) were successfully synthesized and investigated for their cyto-toxic effect on human liver hepatocellular carcinoma cell line (HepG2 cells) by adopting MTT, DNA Ladder, TUNEL assay and qPCR based gene expressions through mRNA quantifications. The TUNEL and DNA ladder assays suggested an insignificant apoptosis in HepG2 cells due to the LFCSNs treatment. Further, the qPCR results also show that the mRNA expressions of cell cycle checkpoint gene p53 and apoptosis related gene (*caspase-9*) was up-regulated, while the antiapoptotic gene *BCl-2* and apoptosis related genes *FADD* and *CAS-3* (apoptosis effecter gene) were down-regulated in the LFCSNs treated cells. The nanospheres that were loaded into the cells confirm their intracellular uptake by light and fluorescent spectro-photometry and microscopy imaging analysis. The loaded nanospheres demonstrate an absolute resistance to photo-bleaching, which were applied for dynamic imaging to real-time tracking *in-vitro* cell migratory activity for continuous 24 and 48 h durations using a time-lapsed fluorescent microscope. These properties of LFCSNs could therefore promote applications in the area of fluorescent protein biolabeling and drug-delivery.

1. Introduction

Over the past decade, mesoporous silica nanoparticles have been the subject of intensive research due to their unique properties that include stable mesoporous structure, tunable pore size, non-toxic, high specific surface area and well modifiable surface. These properties have endowed them with enormous potential applications in the fields of catalysis, drug delivery, biosensing and optically active materials (Luo et al., 2011; Pan et al., 2012; Zhao et al., 2009; Kim et al., 2008; Lai et al., 2008). Several research groups have reported designs of drug sustained/controlled delivery systems based on mesoporous silica materials (Mamaeva et al., 2013; Tang et al., 2012; Zhang et al., 2012; Taylor et al., 2008; Ansari et al., 2011, 2013b; Upadhyay et al., 2014a,b, 2015). However, the main problem of mesoporous silica when used as luminescence

* Corresponding author. Fax: +966 1 4670662.
E-mail address: aneesaansari@gmail.com (A.A. Ansari).
Peer review under responsibility of King Saud University.

ELSEVIER Production and hosting by Elsevier

http://dx.doi.org/10.1016/j.sjbs.2016.08.012
1319-562X

probes is that luminescence measurement is easily affected by non-specific light scattering, such as Tyndall, Rayleigh, and Raman scattering, which then limit the effectiveness of mesoporous silica as luminescence probes for quantitative bioassays (Deng et al., 2010; Mamaeva et al., 2013).

Recently, a method to prepare luminescent functionalized mesoporous core-shell microspheres has been developed by our group and thus established a highly sensitive fluorescent imaging method using microspheres as fluorescence probes (Yang et al., 2008; Yu et al., 2005; Lin et al., 2007; Ansari and Labis, 2012; Ye et al., 2004a). Furthermore, Yang et al. (2008) prepared luminescent functionalized mesoporous silica through Pechini sol–gel process and investigated their applications in drug-delivery systems. Luminescent functionalized core-shell morphology can be used as precursor to produce hollow spheres and thus lower the cost of the precious materials by coating them on inexpensive cores. Core-shell materials can also be used to protect medicines and other materials from dissolution or hydrolysis. Furthermore, surface functionalization of hydrophobic silica nanoparticles is a prerequisite for biomedical applications, not only to render them reasonably water-stable and biocompatible, but also to provide active sites for subsequent functional conjugation with biological or chemical moieties (Yang et al., 2008; Yu et al., 2005; Ansari et al., 2013a; Ansari and Labis, 2012; Ye et al., 2004a,b). In contrast to other non-porous solid nanoparticles, luminescent functionalized core-shell nanospheres offer two different surfaces, *i.e.*, the exterior (particle) and interior pore surfaces. The chemical accessibility to these surfaces of LFCSNs could be tuned by varying their pore diameters and particle sizes. Taking advantage of these characteristics, one can manipulate these materials to interact with cell membranes, sub-cellular organelles, and biological macromolecules, such as proteins and oligonucleotides, for drug/gene delivery and bio-sensor applications (Di et al., 2011; Yang et al., 2008).

In this paper, we present potential effects of synthesized luminescent functionalized core-shell nanospheres on HepG2 cells using different techniques. Our results show that LFCSNs was non-toxic to HepG2 cells as confirmed by cell proliferation MTT, TUNEL, Ladder assay and the gene expression real PCR. Further, we also examined the interaction between the LFCSNs and cells, since LFCSNs–cell biocompatibility and uptake mechanisms play a crucial role in providing preliminary data for use of LFCSNs in both *in-vitro* and *in-vivo* therapeutic or non-invasive imaging purposes. These bioconjugated core-shell nanospheres could raise new possibilities for ultrasensitive and multiplexed imaging of molecular targets in living cells, animal models, and possibly in human subjects.

2. Materials and methods

2.1. Materials

Terbium oxide (99.99%, Alfa Aesar, Germany), Tetraethyl orthosilicate (TEOS, 99% A.R.), C_2H_5OH, HNO_3, NaOH and cetyl-tri-methyl-ammonium bromide (CTAB) was used as starting materials without any further purification. $Tb(NO_3)_36H_2O$ were prepared by dissolving a corresponding oxide in diluted nitric acid. Ultrapure de-ionized water was prepared using a Milli-Q system (Millipore, Bedford, MA, USA). All other chemicals used were of analytical reagent grade.

2.2. Characterization

The X-ray diffraction (XRD) of the powder samples was examined at room temperature using the PANalytical X'Pert X-ray diffractometer equipped with a Ni filter using Cu K_α (λ = 1.54056 Å) radiations as X-ray source. The size and morphology of the sample was inspected using the JEM-2100F (JEOL, Japan) FE-TEM equipped with an energy-dispersive X-ray spectrometer (EDX). The TEM was operated at an accelerating voltage of 200 kV. The sample for TEM was prepared by depositing a drop of a colloidal ethanol solution of the powder sample onto a carbon-coated copper grid.

2.3. Synthesis of LFCSNs

The synthesis of mesoporous SiO_2 nanospheres and their coatings with $Tb(OH)_3$ shell were carried out as reported earlier (Luo et al., 2011; Pan et al., 2012; Zhao et al., 2009; Ansari and Labis, 2012). In a typical process, N-cetyltrimethylammonium bromide (CTAB, 1.00 g, 2.74 mmol) was dissolved in 420 mL of nanopure water/C_2H_5OH (75/25 = W/W) solution. 4.0 mL aqueous solution of 0.2 M NaOH was introduced to the CTAB solution and the temperature of the mixture was maintained at 80 °C. Tetraethyl ortho-silicate (TEOS, 5.00 mL) was added drop-wise to the surfactant solution under vigorous stirring. The mixture was then allowed to react for 2–3 h to give rise to white precipitates. Then, a mixed solution of 0.5 mg CTAB, terbium tris-acetylacetonate trihydrate ($Tb(acac)_33H_2O$) (5 mL) dissolved in 15 mL H_2O/C_2H_5OH (75/25 = W/W) solution was introduced into the foregoing reaction (Ansari et al., 2007). The mixture was continuously stirred overnight at 40 °C. The resulting ternary nanocomposites consisting of $SiO_2@Tb(OH)_3$ core-shells were then isolated by centrifugation and washed with hot de-ionized water to remove the excess CTAB and other reactants and thus avoid their adverse effects on the surface area and on the photoluminescence property of the by-product. For each washing, a sonicator was used to completely disperse the nanospheres in water. Finally, the sample was dried in air to yield the as-synthesized LFCSNs.

2.4. Culture and maintenance of HepG2 cell lines

The HepG2 cell line was purchased from ATCC, USA. The cell line was maintained in 90% Eagle's Minimal Essential Medium (EMEM) containing 10% fetal bovine serum (FBS) and 1% penicillin/streptomycin. The cells were cultured as adherent monolayers (i.e., cultured at ~70–80% confluence) and maintained at 37 °C in a humidified atmosphere of 5% CO_2. The cells were harvested after brief trypsinization.

2.5. MTT assay

Cytotoxicity was determined by the MTT assay (Mossman, 1983). MTT assay is based on the ability of viable cells to reduce the soluble, yellow 3-(4,5dimethyl thiazol-2-yl)-2,5-diphenyl tetrazolium bromide (MTT) into insoluble, blue formazan product. Normally, around 10,000 cells per well were plated in 96-well microtiter plates in a 200 μL of medium. After 24 h, the medium was changed and the cells were treated

with LFCSNs at different concentrations for 24 h. After the exposure time was completed, the medium was aspirated off and 100 μL MTT (0.5 mg MTT/mL) added and incubated for 4 h. The reaction was stopped and formazan crystal thus formed was solubilized by mixing an equal volume of stop mix solution containing 20% sodium dodecyl sulfate (SDS) in 50% N,N-dimethylformamide (DMSO). The plates were placed on a shaker for 15 min for complete solubilization of crystals and then the optical density of each well was determined. The quantity of the formazan product as measured by the amount of 545 nm absorbance was directly proportional to the number of living cells in culture. Each experiment was done in triplicate. The cell viability (%), which is related to control wells containing cell culture medium without nanospheres as a vehicle was calculated by $[A]_{test}/[A]_{control} \times 100$, where $[A]_{test}$ is the absorbance of the test sample and $[A]_{control}$ is the absorbance of control sample. IC_{50} was also calculated. The experiment was carried out as technical and biological triplicates. The results were then expressed as mean ± SEM.

2.6. DNA ladder assay

DNA ladder assay was used to analyze the fragmentation of the genomic DNA as an evidence of apoptosis. This assay protocol was developed by Zhivotosky and Orrenius (2001). In this process, HepG2 cells (1.5×10^6 cells/well) were cultured in 6-well plates for 24 h. The cells were treated with the highest concentration (640 μg/mL) of LFCSNs for 24 h. After the incubation period, the culture medium was aspirated, and the cell layers were trypsinized. The harvested cells were washed twice with phosphate buffer saline (PBS) by centrifugation at 2500 rpm for 5 min. The cell plate was then transferred to a micro-centrifuge tube. 100 μL of lysis buffer (1% TrotonX-100 in 20 mM EDTA, 50 mM tris-HCl, pH 7.5) was added to the cells and incubated for 10 s. The tube was centrifuged (3,000 rpm, 5 min) to obtain the supernatant. 10 μL of 10% SDS solution and 10 μL 50 mg/ml RNase A were added to the pooled supernatant and incubated for 2 h at 56 °C. After incubation 10 μl of 25 mg/ml Proteinase K was added and incubated again for 2 h at 37 °C. Then, 65 μL of 10 M ammonium acetate and 500 μL ice cold ethanol were added and mixed thoroughly. For ethanol precipitation of DNA, the tube was kept at −80 °C for 1 h. After precipitation, the tube was centrifuged at 12,000 rpm for 20 min. The supernatant was discarded and 80% ethanol was added to the DNA pellet. The DNA was vacuum dried. DNA pellet then dissolved in 50 μL TE buffer. 7 μL of DNA solution was mixed with the sample loading dye and the fragmented DNA were resolved in 2% agarose gel.

2.7. TUNEL assay

The DeadEnd® TUNEL assay kit (Promega, Madison, WI) was used to analyze apoptosis in a time-dependent manner. The manufacturer's instructions were followed with slight modifications. In this process, HepG2 cells (1.5×10^6 cells/well) were cultured in 6-well plates to study the apoptosis in adherent cells. The cells were treated with the highest concentration (640 μg/mL) of nanospheres for 24 h. After the incubation period, the culture medium was aspirated, and the cell layers were trypsinized. The trypsinized cells were reattached on 0.01% polylysine-coated slides, fixed with 4% methanol-free formaldehyde solution, and stained according to the DeadEnd fluorometric TUNEL system protocol (Wang et al., 2004). The stained cells were observed using a Carl-Zeiss (Axiovert) epifluorescence microscope using a triple band-pass filter. To determine the percentage of cells undergoing apoptosis, 1000 cells were counted in each experiment (Hasan et al., 2011). The experiment was carried out as technical and biological triplicates. The results were then expressed as mean ± SEM.

2.8. cDNA synthesis and qPCR for apoptosis related gene expression

The HepG2 cells were cultured in six-well plates at a density of 1.5×10^5. After 24 h of adhesion, the culture media were aspirated off and the cells were treated with the nanospheres. After 24 h of incubation, the media were removed and the treated cells were washed with ice-cold PBS. Fastlane Cell cDNA kit (QIAGEN, Germany) was used to prepare cDNA directly from the cultured cells, according to the manufacturer's instructions. The mRNA levels of *tp53*, *CAS-3*, *-9 FADD* and *BCl-2* as well as the reference gene, *GAPDH*, were assayed using gene-specific SYBR Green-based QuantiTect Primer assays (QIAGEN, Germany). Real-time PCR reactions and analyses were performed on in Applied Biosystems 7500 Fast (Foster City, CA, USA). The PCR reaction conditions, reaction volumes and calculation of fold change in expression were chosen to be exactly the same as published earlier (Hasan et al., 2011).

2.9. Cellular uptake and in-vitro imaging studies

Fluorescent microscopy was employed to examine the cellular uptake and distribution changes of LFCSNs into HepG2 cells. The HepG2 cells approximately (1×10^5) were cultured in a 6 well plate in a medium made up of EMEM and treated with of LFCSNs for 24 and 48 h with technical triplicates, Untreated control and treated cells were observed under inverted microscope (Carl Zeiss, Deutschland). For each experiment, nuclei from 10 random fields of well were examined at 200× magnification. Acridine Orange (AO) fluorescent dye was used.

AO is taken up by both viable and nonviable cells and emits green fluorescence if intercalated with double stranded nucleic acid (DNA) or red fluorescence if bound to single stranded nucleic acid (RNA). Ethidium bromide is taken up only by nonviable cells and emits red fluorescence by intercalation into DNA. Four types of cells can be distinguished according to the fluorescence emission and the morphological aspect of chromatin condensation in the stained nuclei. Viable cells have uniform bright green nuclei with an organized structure. Early apoptotic cells (which still have intact membranes but have started to undergo DNA cleavage) have green nuclei, but perinuclear chromatin condensation is visible as bright green patches or fragments. Late apoptotic cells have orange to red nuclei with condensed or fragmented chromatin. Necrotic cells have uniformly orange to red nuclei with a condensed structure. An amount of 20 μL of dye mixture (10 μL/mg AO and 10 μL/mg EB in distilled water) was mixed with 100 μL distilled water and added to each well.

4′-6-Diamidino-2-phenylindole (DAPI) is known to form fluorescent complex with natural double-stranded DNA,

showing fluorescence specificity for adenine-thymine (AT), and adenine-uracil (AU) clusters. Because of this property DAPI is a useful tool in various cytochemical investigations. When DAPI binds to DNA, its fluorescence is strongly enhanced, which is interpreted in terms of a highly energetic and intercalative type of interaction, but there is also evidence that DAPI binds to the minor groove, stabilized by hydrogen bonds between DAPI and acceptor groups of AT and AU base pairs. The membrane permeable fluorescent dye DAPI (2 μg/mL) (Sigma Aldrich), which binds to chromatin of cells, is added to the fixed cells.

Propidium iodide (PI) binds to DNA by intercalating between the bases with little or no sequence preference and with a stoichiometry of one dye per 4–5 base pairs of DNA. PI also binds to RNA, necessitating treatment with nucleases to distinguish between RNA and DNA staining. Once the dye is bound to nucleic acids, its fluorescence is enhanced 20- to 30-fold, with the fluorescence excitation maximum is shifted ~30–40 nm to the red. PI is membrane impermeant and generally excluded from viable cells. PI is commonly used for identifying dead cells in a population. 50 μL of 50 μg/mL PI solution was added to each well. Incubated for 15 min and the cells were examined by an inverted Axio Observer.D1 + Apo Tome (Carl Zeiss, Deutschland). Apoptotic cells in each fluorescent dye staining were identified by condensation and fragmentation of nuclei. For each experiment, nuclei from 10 random fields of well were examined at 200× magnification (Ansari et al., 2013a,b).

3. Results and discussion

Typically, the monodispersed mesoporous silica nanospheres as shown in Fig. 1 were synthesized via the modified Stöber method (Luo et al., 2011; Pan et al., 2012; Zhao et al., 2009). These nanospheres will act as a morphology-determining template for the LFCSNs, and the uniformity of these cores will be responsible for the sharp distribution of final particle sizes. Fig. 1b shows the absorption spectra of the as-synthesized silica nanospheres, which matched well with other literature reports (Yu et al., 2007).

As shown in the TEM images of Fig. 2a, a uniform thin layer (~10 nm) of terbium hydroxide is formed around the surface of silica core nanosphere. In this reaction, CTAB was selected as the organic template for the deposition of terbium hydroxide shell around the silica nanosphere. Here, the CTAB serves not only as the stabilizing surfactant for the transfer of hydrophobic $Tb(OH)_3$ nanocrystals to the aqueous phase but also as the organic template for the formation of mesopores in the sol–gel reaction. The cationic surfactant molecule, CTAB, plays two important roles in this process; (i) solubilization of hydrophobic silica nanospheres into aqueous solutions and (ii) templating the nanometer-sized pore formation. In the first step, CTAB molecules in aqueous solution stabilize the oil droplets leading to the formation of an oil-in-water microemulsion after the formation of silica nanospheres. Consequently, CTAB molecules directly interact with the silica nanospheres surface through hydrophobic interactions. The alkyl chains of the CTAB and the silica nanospheres surface ligands intercalate into each other, rendering the CTAB cationic head group (quaternary amine) facing outward and the silica nanospheres-CTAB complex water-soluble. In the second step, when added with terbium chelate into this solution, terbium chelate dissociates due to the presence of a strong base in the solution media that is formed as terbium hydroxide shells on silica nanospheres surface. Thus, the CTAB acts as templates for mesopore formation (also known as porogen). Systematic investigation of core-shell on nanospheres (Lin et al., 2007; Ansari and Labis, 2012; Ansari et al., 2013a,b; Ye et al., 2004a,b) have suggested a three-stage reaction: (i) hydrolysis of alkoxy-silanes and formation of silica oligomers, (ii) formation of silica/CTAB primary nanospheres, and (iii) hydrolysis of terbium chelate in the presence of strong base and mesopore growth of shell via aggregation of the hydroxide particles on the silica nanospheres surface. The excess surfactant molecules can be removed by repeated rinsing with ethanol after the reaction.

The LFCSNs prepared by this method have two main advantages as compared to the luminophore-doped silica nanospheres. One is that the fluorescent Tb^{3+} hydroxide layer in the nanospheres is highly stable without dye leaking during the washing, biolabeling and bioassay processes since the hydroxide particles in the nanospheres exist by covalently interacting with the silica network. The other is that free hydroxyl groups that are directly introduced to the surface of the nanospheres by hydrolysis of Tb^{3+} chelate into terbium hydroxide form free hydroxyl groups in the nanospheres preparation. These hydroxyl groups are directly available for biolabeling of the nanospheres without a tedious surface activation procedure.

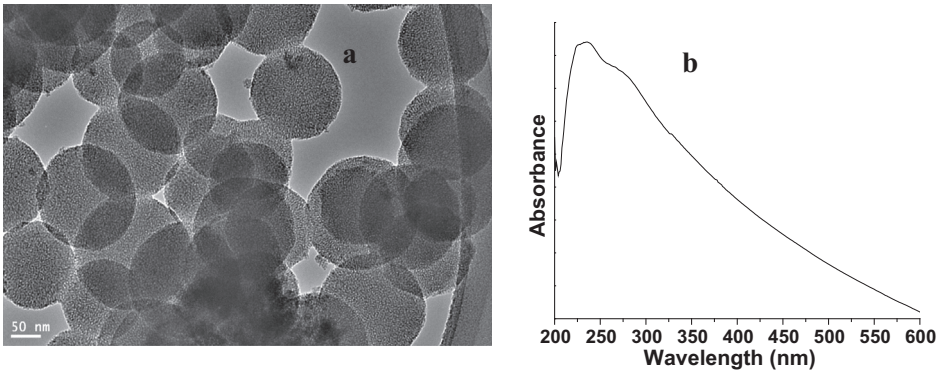

Figure 1 (a) FE-TEM micrograph and (b) UV/Vis absorption spectrum of the pure silica nanospheres.

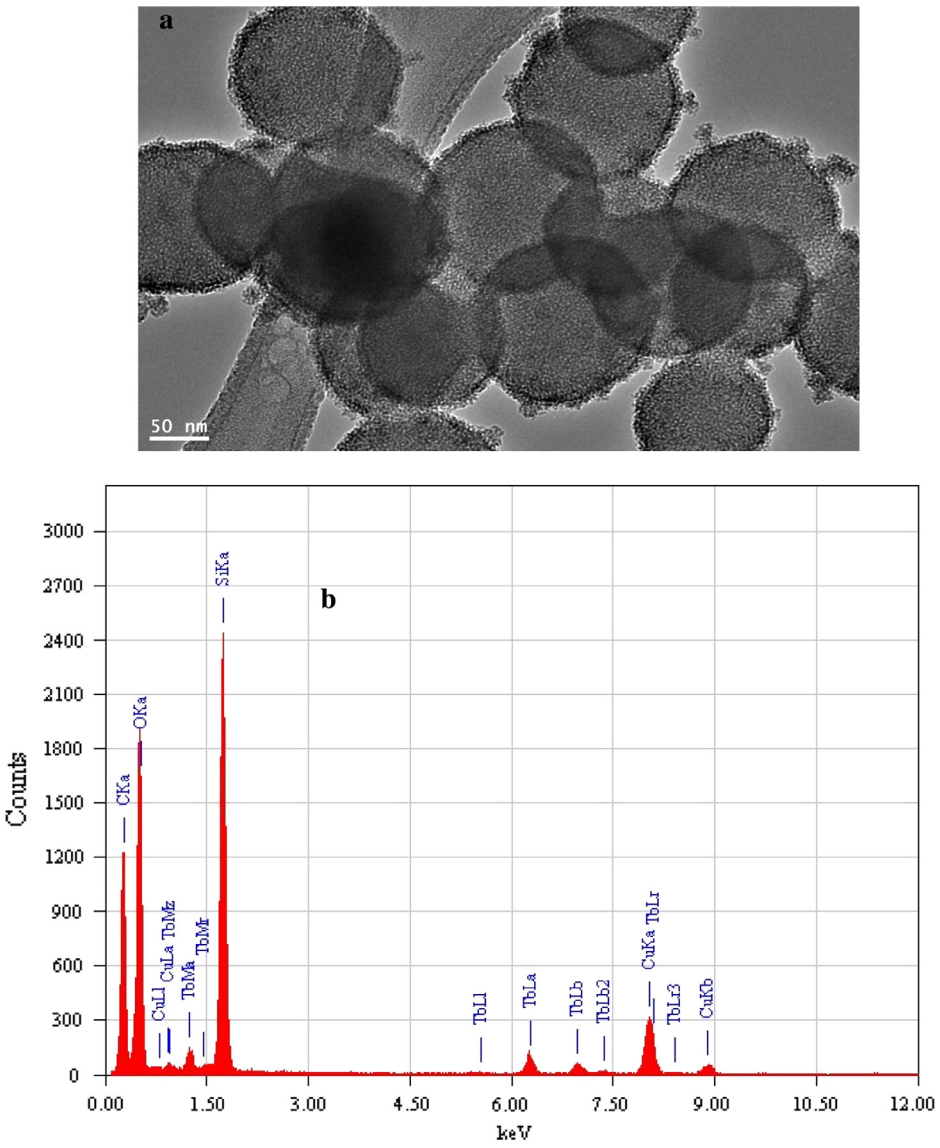

Figure 2 (a) High-resolution FE-TEM micrograph of the LFMCSNs and (b) EDX study of the LFMCSNs.

These nanospheres were characterized by different spectroscopic techniques. The uniform terbium hydroxide coating on the surface renders them water soluble and thus compatible with biological applications. In this study, we have demonstrated then the use of these core-shell nanospheres as a new fluorescent cell tracker probe for superior *in-vitro* and *in-vivo* imaging due to their unique optical properties.

Fig. 2 represents the FE-TEM micrographs of the mesoporous core-shell LFCSNs. The TEM image illustrates a well-separated luminescent mesoporous silica coated with Tb $(OH)_3$ nanospheres that are almost spherical with a mean diameter of 125 nm. Although the TEM sample exhibits that the terbium hydroxide layer had been overlapped on the surface of mesoporous silica nanospheres, the contrast between the dark-black terbium hydroxide layer (10–12 nm thick) and the light-gray amorphous silica (110 nm in diameter) is apparent. It thus demonstrated that all nanospheres are single nanospheres. This can be further confirmed by the high-resolution TEM micrographs.

The energy-dispersive X-ray (EDX) spectrum of the synthesized core–shell nanospheres also supported the formation of terbium hydroxide layer around the surface of silica core-nanospheres (Fig. 2b). The detection of strong peaks of terbium (Tb), silicon (Si) and oxygen (O) elements in the EDX spectrum is a strong indication of a construction core-shell structure. Note however that the C and Cu signals were from the Cu grid (substrate) on which the sample was deposited. No other impurities are evident in the figure, implying that the resulting luminescent functionalized core–shell nanospheres are pure in chemical composition.

Fig. 3a exhibits the wide-angle XRD pattern of LFCSNs as-synthesized by sol-gel process. The XRD spectrum of the nanospheres shows only a broad diffraction located at ~30–48°. No sharp diffraction peaks were observed, which might denote a crystalline structure. Thus, no crystalline phase of Tb^{3+} ions was detected in the diffraction. The broad peak measured by wide-angle XRD is either attributed to the existence of amorphous silica (Card No. JCPDS 29–0085) compo-

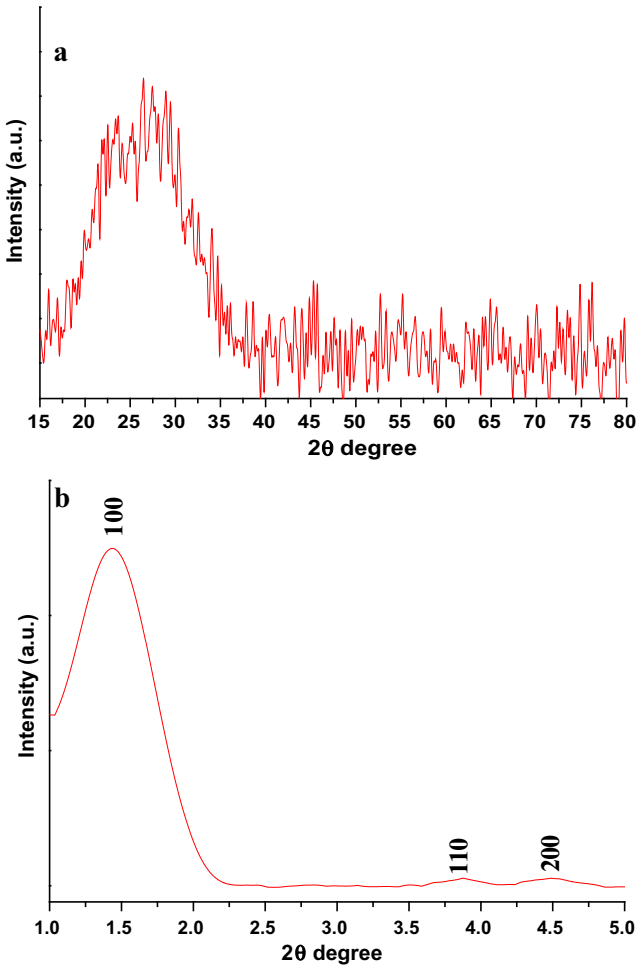

Figure 3 (a) Wide-angle X-ray diffraction pattern and (b) small-angle X-ray diffraction pattern of the LFMCSNs.

nents or to the ultra-small crystalline nature of the materials, where diffraction peaks cannot be well resolved (Yang et al., 2008; Yu et al., 2005). Therefore, it can be argued that the luminescent functionalized (Tb^{3+}) in the silica framework expands the nanopores and rearranges the Si–O–Si network structures without any involvement of impurities. This is in accord with the previous literature reports (Yang et al., 2008; Ye et al., 2004a; Yu et al., 2007; Ai et al., 2009; Santra et al., 2001). It therefore confirms that LFCSNs are non-crystalline material and Tb(β-diketonates)$_3$3H_2O chelate molecules in the nanospheres are either in a non-crystalline or in an ultra small crystalline state (Yu et al., 2007; Ai et al., 2009; Ansari et al., 2013a,b; Santra et al., 2001).

Small-angle XRD pattern is similarly obtained for the synthesized LFCSNs. And as seen in Fig. 3b, a strong low-angle (100) diffraction peak is shown at about $2\theta = 1.4°$ with two small peaks indexed as (110) and (200) which could be associated with a 2D hexagonal meso-structure (p6mm) thus conforming their highly ordered meso-structure.

3.1. In-vitro cytotoxicity assay

To provide comprehensive results about the potential applications of synthesized LFCSNs for non-invasive imaging purposes, it is essential to measure the cytotoxicity of the synthesized material. As shown in Fig. 4, the cytotoxicity profile of composite particles is determined in human hepatoblastoma (HepG2) cells using a MTT assay. HepG2 cells were treated with different concentrations of LFCSNs for 24 h, to determine the effect of dose dependency on incubation as well as on concentration of the LFCSNs. Various concentrations from 0, 5, 10, 20, 40, 80, 160, 320 and 640 μg/mL of LFCSNs were exposed at HepG2 cells for 24 h. The dose-dependent HepG2 cells viability at 24 h was 100, 82.5, 82, 80.9, 76.1, 68.7, 67.8, 65.1 and 53.5%, respectively. The cytotoxic effects of the LFCSNs on mitochondrial activity of cells were increased in relation to the increasing LFCSNs concentration. More than 80.1% cells viabilities were observed in a wide range of concentrations (i.e., from 5 to 20 μg/mL) after a 24-h incubation period. When the LFCSNs concentration was increased to 320 μg/mL, the cell viability still remained above 65% (Fig. 4). The IC_{50} was not achieved even up to the highest concentration of 640 μg/mL. The cell viability at 640 μg/mL (53.5%) indicated evidence of mild toxicity at the highest concentration of LFCSNs. These observed results suggested that LFCSNs at upto a concentration of 640 μg/mL can be considered to have low cytotoxicity. This concentration was used for analysis of cyto-toxicity parameters. It is worth to mention that the surface functional groups of LFCSNs may have impact on the cell viability. Yu et al., 2009 reported that SiO_2 nanoparticle (118 nm) was not cytotoxic at 100 μg/mL against mouse keratinocyte. The results of this study have revealed that more than 30% cells are dead at 100 μg/mL, whereas, after exposing similar LFCSNs concentrations for 48 and 72 h, the number of viable HepG2 cells decreased sharply from 82% to 40% of untreated cells, respectively (data not shown here). Hence, it can be suggested that the formation of $Tb(OH)_3$ shell over SiO_2 core increases the number of cytotoxic particles. Although the hydroxyl groups of the luminescent terbium hydroxide are readily subjected to further biomodification, the positively charged surface provides a suitable functional group to allow further conjugation by active biomolecules, which may lead to nonspecific adsorption on cell mem-

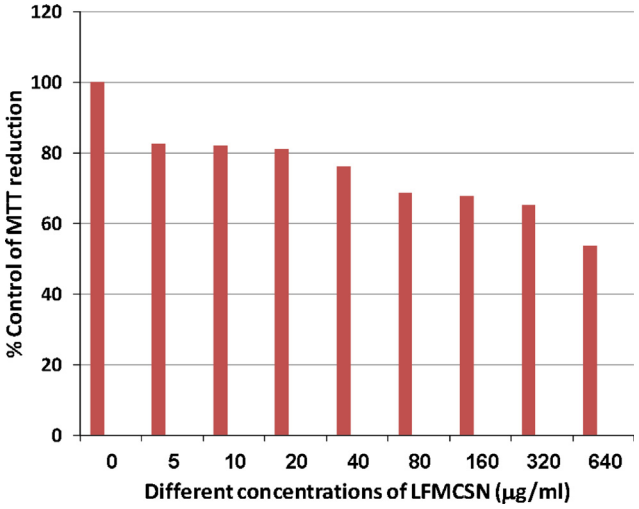

Figure 4 Evaluation of cytotoxicity by MTT assay and determination of IC_{50} of LFCSNS against the HepG2 liver cancer cell line.

branes for further biological applications. In this assay, no significant toxicity was observed over the entire concentration range tested during the 48 h of the experiment. These results therefore suggest that LFCSNs could potentially serve as optical contrast agents for bioimaging.

3.2. DNA ladder assay for genomic DNA fragmentation as evidence of apoptosis

The HepG2 cells were exposed to LFCSNs at the highest concentrations of 640 μg/mL for 24 h. DNA ladder assay was performed according to the protocol developed earlier by Zhivotosky and Orrenius (2001) with slight modification to investigate the fragmentation of genomic DNA. Although we subjected the LFCSNs to extensive DNA treatment followed by electrophoresis on 1% agarose gel (Fig. 5), we have not observed any fragmentation of the genomic DNA as observed by the agarose gel electrophoresis assay imaging shown in Fig. 5.

3.3. TUNEL assay for the DNA strand break as evidence of apoptosis

The genotoxic potentiality of these LFCSNs along with HepG2 cells was further supported by apoptosis assay/TUNEL assay (dUTP nick-end labeling) as shown in Fig. 6. TUNEL assay is an efficient combination of molecular biology and morphological observation through microscopy. It is used largely for the quantification of apoptotic cells (Hasan et al., 2011). We performed the TUNEL assay on HepG2 cells in the presence of these LFCSNs according to published literatures (Patra et al., 2009; Chen et al., 2006). TUNEL assay was employed to find out cell death after treatment with LFCSNs due to the induction of apoptosis. as we have already demonstrated in cell viability tests using a trypan blue dye exclusion test, cell proliferation assay (MTT assay) and apoptosis assay (Ladder assay). In the previous paragraph, we observed similar cell apoptosis results in the TUNEL assay. In the TUNEL assay of HepG2 cells treated with LFCSNs for 24 h, we have found a few green TUNEL positive nuclei indicating no apoptosis. The representative photographs of apoptosis assay of HepG2 cells treated with LFCSNs (640 μg/mL) are presented in Fig. 6 This finding suggests that the LFCSNs have caused very little apoptosis in HepG2 cells. These results support the reported literature (Nakamura et al., 1997; Palasz and Czekaj, 2000), where Nakamura et al. (1997) observed mild toxicity of the lanthanide ions in blood samples. On the other hand, Patra et al. (2009) also observed a high concentrations of europium hydroxide nanorod (125 mg kg^{-1} - day^{-1}) in various parts (liver, kidney, and lungs) of mice, but

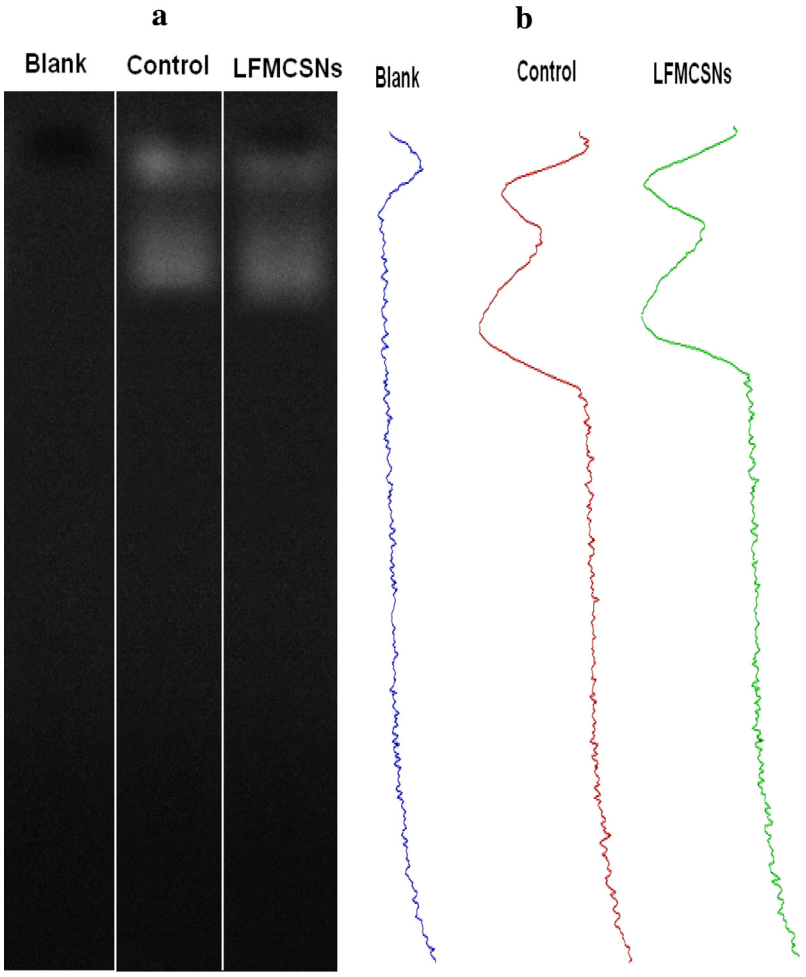

Figure 5 DNA ladder assay: Agarose gel electrophoresis of genomic DNA for visualization of their fragmentation as evidence of genotoxicity with respect to control (a) and genomic DNA band intensity peaks (b).

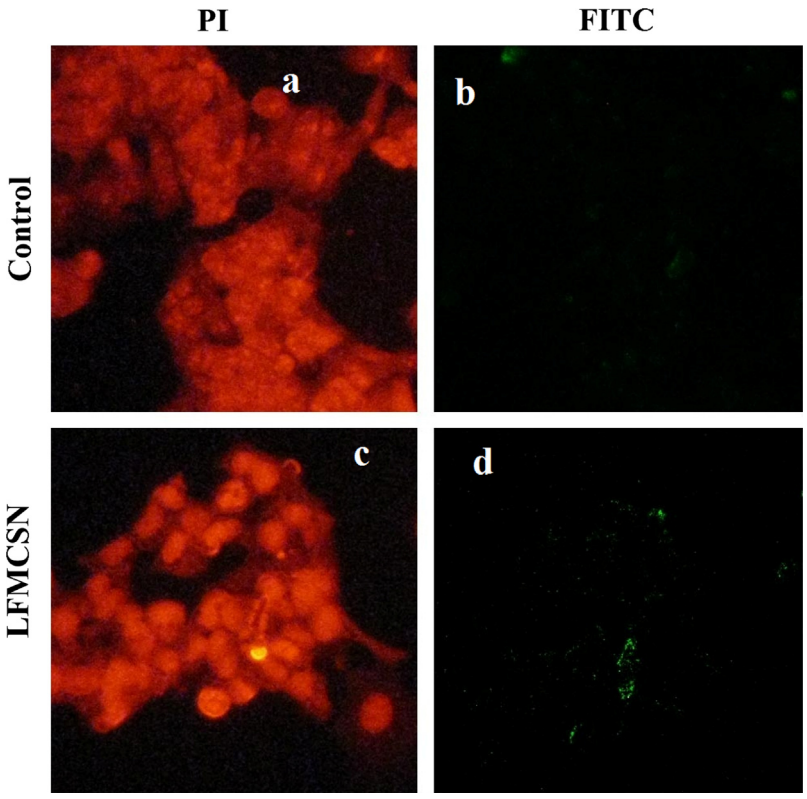

Figure 6 TUNEL assay after 24 h incubation of HepG2 cells against LFCSNS. Red fluorescence is due to Propidium Iodide staining and observed under green filter while green fluorescence is due to FITC staining and observed under blue filter. Observations done at 400× magnification.

didn't show any lethal toxicity; and even in long-term toxicity studies, there was no death of mice using high concentrations of inorganic nanorods. Further they remained much longer in the organs for more than 60 days (i.e. a 100% survival rate). Our observed results suggest that the LFCSNs at lower concentrations of up to 10 μg/ml modulate the antioxidant enzymes levels, whereas, at higher concentrations, the cellular DNA repair machinery may be adversely affected. Consequently, some cells of unrepaired DNA damage were detected upon using higher concentrations of LFCSNs due to the production of reactive oxygen species through non-bonded hydroxyl groups with genomic DNA molecules, which were present on the surface of the LFCSNs.

Similarly, for the toxicity study we did not find any significant difference in Ladder and TUNEL assay examination results even at highest concentration of LFCSNs up to 640 μg/ml. Our observed results demonstrated no cell apoptosis as seen in Fig. 6d. It is reported that the nanospheres could directly bind to DNA or repair enzymes leading to the generation of strand breaks (Hartwig, 1998; Reeves et al., 2008). As a result, negatively charged DNA becomes attached electrostatically to the positively charged (owing to acidic condition) quaternary nitrogen atom of the surface-modified terbium hydroxide coated silica nanospheres. However, there are contradicting results in literatures on the exposure with different nanoparticles at different stages of embryo development and also with the differences in the experimental models (Challier et al., 1973; Bosman et al., 2005). Thus, the extent of induced genetic damage, and risk assessment of the nanomaterials and nanoproducts should be assessed further prior to their wider applications in spite of their apparent extraordinary advantages.

3.4. Determination of differential expression of apoptosis related genes by qPCR

To verify the mRNA results, we further examined the expression levels of several apoptosis-related genes at protein levels in LFCSNs exposed HepG2 cells using Real Time PCR assay. Generally, BCL-2, P53, CAS-3, -8, -9 and FADD are major proteins which are involved in apoptosis. It is known that apoptosis is a key process in cancer development and progression. The ability of cancer cells to avoid apoptosis and continue to propagate is one of the basic characteristics of cancer and is a major target of cancer-therapy (Ashkenazi, 2002). In our case, we did not observe any LFCSNs induced apoptosis in human liver cancer cells. The relative quantification of *BCL-2*, *P53*, *CAS-3*, *-9* and *FADD* mRNA levels were performed and their gene-expression changes results are summarized in Fig. 7. The real-time PCR results suggests that the expressions of both mRNA and protein levels of cell cycle checkpoint gene P53 and pro-apoptotic genes CAS-9 are significantly up-regulated, whereas the expression of anti-apoptotic gene *BCL-2*, *CAS-3* and *FADD* are significantly down-regulated ($P \leqslant 0.05$) in HepG2 cells due to exposure of LFCSNs. Previous related investigations shows that there was a strong association between decreased surviving levels and induction of apoptosis in cancer cells (Li and Ma, 2010;

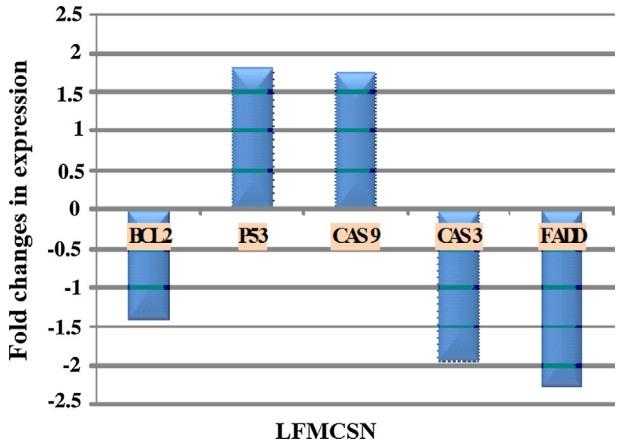

Figure 7 Comparative study of apoptosis related gene expressions as fold change (ratio of target: reference gene) in HepG2 cells after exposure of LFCSNs up to 24 h.

Zaffaroni et al., 2007). And that anti-apoptosis function of surviving also seemed to be related to the ability to disturb the function of caspases (Zaffaroni et al., 2007). Supporting these findings, our results show that LFCSNs inhibit the expression of surviving along with the activation of CAS-3 and CAS-9 enzymes. Furthermore, the expression of antiapototic protein BCL-2 was significantly lower, while the expression of pro-apoptotic protein FADD was significantly higher in cells exposed to LFCSNs, suggesting that these proteins could be excellent molecular biomarkers to assess the genotoxicity response of nanomaterials (Liu and Martin, 2001). The P53 protein is regarded as the master guardian of the cell and is able to activate cell cycle checkpoints, DNA repair and apoptosis (Liu and Martin, 2001; Bartek and Lukas, 2001). The CAS-9 activation is dependent on the release of cytochrome c from mitochondria to form the apoptosome, which in turn activates CAS-3. In this study, significant higher activity of CAS-3 and CAS-9 enzymes was observed that suggest an involvement of caspase cascade in LFCSNs-induced apoptosis in HepG2 cells (Fig. 7). These findings further suggest that there were no significant apoptosis caused by the core-shell nano-spheres after 24 h treatment.

3.5. Cellular uptake or fluorescent probe for in-vitro imaging

To confirm the potential use of LFCSNs as luminescent biological labels, we conducted an *in-vitro* biological experiment using human liver cancer (HepG2) cells. This quantitative evaluation of the cellular uptake and optical detection of molecular interactions play a vital role in clinical biology. It is essential to see how luminescent bio-probe intimately associates with, or is internalized by, the cells. To demonstrate the efficacy of the LFCSNs to serve as a luminescent bio-probe under biological conditions, an *in-vitro* imaging experiment is performed with HepG2 cells. The HepG2 cells and the LFCSNs are fluorescently labeled by encapsulation of the hydrophobic dyes, such as AO/EtBr (Fig. 8C and C′), DAPI (Fig. 8D and D′), PI (Fig. 8E and E′) to identify the cell nucleus. All images were taken under the identical conditions and the cell nucleus were stained green with AO/EtBr, blue with DAPI and red with PI, respectively. These hydrophobic dyes are stably encapsulated onto the hydrophobic surface of the LFCSNs to visualize the transport of LFCSNs into the cells. Optical fluorescence microscopy images were used to study the cellular uptake of the cells and luminescent nanomaterials by monitoring the morphological changes (Fig. 8A and A′ and B and B′). Fig. 8 displays the phase-contrast microscopic images of the transfected HepG2cells in the presence of LFCSNs as captured by a fluorescent microscope. As shown in Fig. 8 A through E, both dye-labeled cells (data not shown here) and dye-labeled LFCSNs display a relatively uniform fluorescence distribution in the cytoplasmic compartment. No obvious morphological abnormalities of the cells were observed, indicating that the LFCSNs are well tolerated by the cells (Fig. 9). Fluorescence within the nuclei was significantly reduced. This suggests that LFCSNs indeed carried the dye upto the cells efficiently, and thus indicating an efficient internalization of these colloids by the cells. Furthermore, it appeared that the fluorescence in the cells incubated with dye encapsulated cells (Fig. 8) is less intense than in those treated with dye-encapsulated LFCSNs (Fig. 8).

In this assay, cells were labeled with LFCSNs via charge interaction between the positive surface hydroxyl terminal groups and negatively charged cell membrane. The images show the attached LFCSNs onto the surface of the cells. While the binding of the LFCSNs to the surface of the cells is rapid and extensive fluorescence can be detected within an hour, uptake into cells through the internalization of the bound receptor– LFCSNs complex is a much slower process and can usually be detected in significant amount only after 24–48 h of incubation. In addition, non-specific uptake of LFCSNs (640 μg/ml) is likely due to the high incubation concentration (1×10^5 ml) and extended incubation times (24 h). After incubation 24 h of HepG2 cells with the fluorescently labeled LFCSNs, the cells were washed, cleaved and centrifuged with PBS to remove the colloids and then replenished with fresh serum-free medium. The successful fluorescent labeling of the cells with LFCSNs was observed by the green emission in comparison with control cells. The emission of the probe localization in the cell cytoplasm, most likely within the endosomal or lysosomal compartments, demonstrates their ability to serve as optical imaging bioprobes. In addition, after incubation with the LFCSNs, no changes in cell morphology or other visual signs of cyto-toxicity were observed in the phase contrast images as shown in Fig. 8. The cells grew with normal fibroblast-like morphologies after co-labeling with the particles and dyes for cell nuclei counterstaining. It can be observed that the transfected HepG2 cells became quite bright owing to the strong fluorescence emitted from LFCSNs distributed in cytosol, while the untreated cells remain dark, suggesting that a large amount of LFCSNs were internalized into the cells. After 24 h transfection, most LFCSNs uptake appeared in endosomal compartments; while some complexes have already successfully escaped from the endosome in such a short time (Fig. 8(A–E)). With both prolonged incubation time and increased concentration of LFCSNs, stronger fluorescence emissions without any cell auto-fluorescence can be observed (Figs. 8 and 9), which show that the cellular uptake of LFCSNs is both time- and dose-dependent. After staining with AO/EtBr and PI and then images by the optical fluorescence microscope, the dead cells were shown in red and the live cells were shown in green as depicted in Fig. 9. In addition, photoluminescence of LFCSNs did not show any decrease in

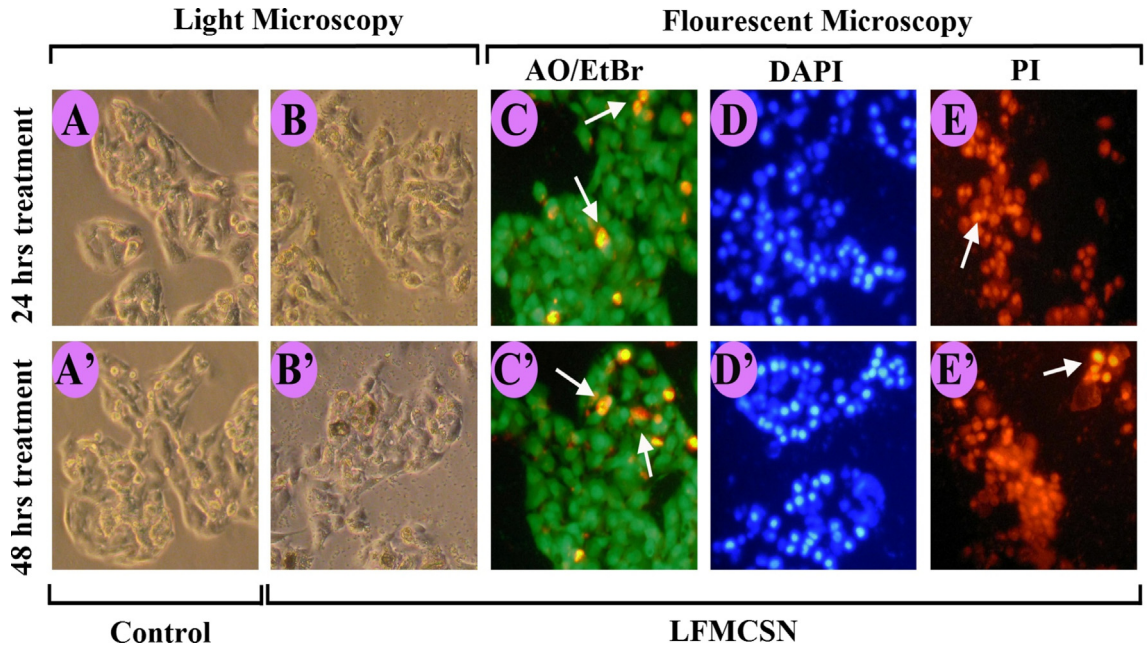

Figure 8 Light and fluorescent microscopy of HepG2 cells LFCSNS treated after 24 h (A–E) and 48 h (A′–E′). Cell colonies are intact in untreated controls (A and A′). Disturbance in colonies structure is evident from light microscopy (arrows in B and B′). Early and late apoptotic cells are visible through AO/EtBr fluorescent staining (C and C′). Nuclear fragmentation and blebbing can be observed (arrows in D and D′). Fragmentation of nuclei and micronucleus is visible (arrows in E and E′).

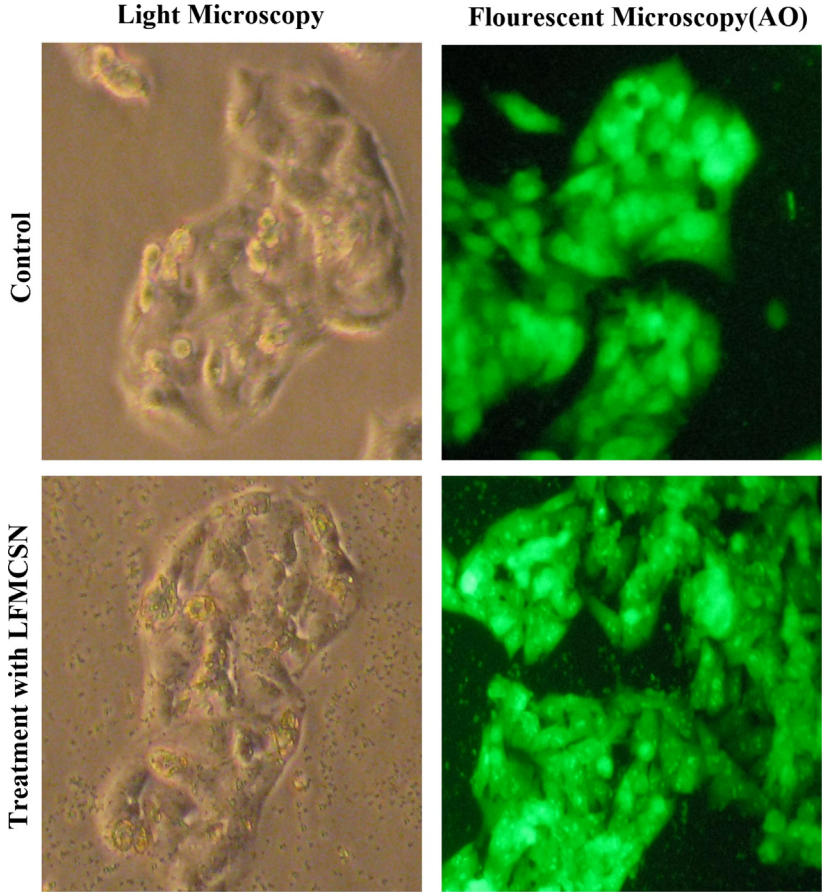

Figure 9 *In-vitro* light and fluorescent microscopy (acridine orange) of human HepG2 cells interaction with LFCSNS treated and control after 24 h.

tendency upon observation for several minutes (data not shown here). These results merit promise in the application of LFCSNs as an excellent luminescent probe with low auto-fluorescence and high photo-stability for cellular bio-imaging.

4. Conclusion

The toxic potentiality of the synthesized luminescent functionalized core-shell nanospheres was investigated and further applied for cellular uptake studies. The synthesized nanospheres were non-toxic to HepG2 cells as observed by apoptosis assay. These cells have survived reasonably well (< 50%) even at the highest concentration used in this study. The presence of a $Tb(OH)_3$-shell layer on the surface of the silica nanosphere was highly favorable, because it can reduce the toxic effect and at the same time enhance the luminescent properties of the nanospheres. The advantages of the LFCSNs in cellular uptake or biolabeling were their easy availability in spherical morphology and their wide applicability. These obtained results support the potential use of LFCSNs in both cellular and animal imaging systems. Considering the chemical inertness and biocompatibility of silica, this method could provide a new platform for nonviral gene delivery as well as cellular bioimaging. This system provides a new dimension for the development of effective diagnostic and therapeutic agents. Future investigations could provide more understanding on the relationship between surface properties and cellular uptake, translocation, metabolism, oxidative effects and other biological effects of controlled size LFCSNs *in-vivo* and *in-vitro*.

Acknowledgement

This project was funded by National Plan for Science, Technology and Innovation (MAARIFAH) King Abdulaziz City for Science and Technology, Kingdom of Saudi Arabia, award Number (13-Bio1246-02).

References

Ai, K., Zhang, B., Lu, L., 2009. Europium-based fluorescence nanoparticle sensor for rapid and ultrasensitive detection of an anthrax biomarker. Angew. Chem. Int. Ed. 48, 304–308.

Ansari, A.A., Alam, M., Labis, J.P., Alrokayan, S.A., Shafi, G., Hasan, T.N., Syed, N.A., Alshatwi, A.A., 2011. Luminescent mesoporous $LaVO_4:Eu^{3+}$ core-shell nanoparticles: synthesis, characterization, biocompatibility and their cytotoxicity. J. Mater. Chem. 21, 19310–19316.

Ansari, A.A., Hasan, T.N., Syed, N.A., Labis, J.P., Parchur, A.K., Shafi, G., Alshatwi, A.A., 2013a. *In-vitro* cyto-toxicity, genotoxicity, and bio-imaging evaluation of one-pot synthesized luminescent functionalized mesoporous $SiO_2@Eu(OH)_3$ core-shell microspheres. Nanomed.: Nanotechnol. Biol. Med. 9, 1328–1335.

Ansari, A.A., Labis, J.P., 2012. One-pot synthesis and photoluminescence properties of luminescent functionalized mesoporous $SiO_2@$-$Tb(OH)_3$ core–shell nanospheres. J. Mater. Chem. 22, 16649–16656.

Ansari, A.A., Labis, J.P., Aldwayyan, A.S., Hezam, M., 2013b. Facile synthesis of water-soluble luminescent mesoporous $Tb(OH)_3@SiO_2$ core-shell nanospheres. Nanoscale Res. Lett. 8, 163–167.

Ansari, A.A., Singh, N., Khan, A.F., Singh, S.P., Iftikhar, K., 2007. Solvent effect on optical properties of hydrated lanthanide tris-acetylacetone. J. Lumin. 127, 446–452.

Ashkenazi, A., 2002. Targeting death and decoy receptors of the tumor-necrosis factor super family. Nat. Rev. Cancer 2, 420–430.

Bartek, J., Lukas, J., 2001. Pathways governing G1/S transition and their response to DNA damage. FEBS 490, 117–122.

Bosman, S.J., Nieto, S.P., Patton, W.C., Jacobson, J.D., Corselli, J.U., Chan, P.J., 2005. Development of mammalian embryos exposed to mixed-size nanoparticles. Clin. Exp. Obstet. Gynecol. 32, 222–224.

Challier, J.C., Panigel, M., Meyer, E., 1973. Uptake of colloidal 198Au by fetal liver in rat, after direct intrafetal administration. Int. J. Nucl. Med. Biol. 1, 103–106.

Chen, J.P., Patil, S., Seal, S., McGinnis, J.F., 2006. Rare earth nanoparticles prevent retinal degeneration induced by intracellular peroxides. Nat. Nanotechnol. 1, 142–150.

Deng, Y., Cai, Y., Sun, Z., Liu, J., Liu, C., Wei, J., Li, W., Liu, C., Wang, Y., Zhao, D., 2010. Multifunctional mesoporous composite microspheres with well-designed nanostructure: a highly integrated catalyst system. J. Am. Chem. Soc. 132, 8466–8473.

Di, W., Ren, X., Zhao, H., Shirahata, N., Sakka, Y., Qin, W., 2011. Single-phased luminescent mesoporous nanoparticles for simultaneous cell imaging and anticancer drug delivery. Biomaterials 32, 7226–7233.

Hartwig, A., 1998. Carcinogenicity of metal compounds: possible role of DNA repair inhibition. Toxicol. Lett. 102–103, 239–355.

Hasan, T.N., B, L.G., Shafi, G., Al-Hazzani, A.A., Alshatwi, A.A., 2011. Anti-proliferative effects of organic extracts from root bark of juglans regia L. (RBJR) on MDA-MB-231 human breast cancer cells: role of Bcl-2/Bax, caspases and Tp53. Asian Pac. J. Cancer Prev. 12, 525–530.

Kim, J., Kim, H.S., Lee, N., Kim, T., Kim, H., Yu, T., Song, I.C., Moon, W.K., Hyeon, T., 2008. Multifunctional uniform nanoparticles composed of a magnetite nanocrystal core and a mesoporous silica shell for magnetic resonance and fluorescence imaging and for drug delivery. Angew. Chem. Int. Ed. 47, 8438–8441.

Lai, C.W., Wang, Y.H., Lai, C.H., Yang, M.J., Chen, C.Y., Chou, P. T., Chan, C.S., Chi, Y., Chen, Y.C., Hsiao, J.K., 2008. Iridium-complex-functionalized Fe_3O_4/SiO_2 core/shell nanoparticles: a facile three-in-one system in magnetic resonance imaging, luminescence imaging, and photodynamic therapy. Small 4, 218–224.

Li, H.L., Ma, A.N., 2010. Induction of apoptosis of non-small cell lung cancer by a methylated oligonucleotide targeting survivin gene. Cancer Gene Ther. 17, 441–446.

Lin, Y.S., Hung, Y., Lin, H.Y., Tseng, Y.H., Chen, Y.F., Mou, C.Y., 2007. Photonic crystals from monodisperse lanthanide-hydroxide-at-silica core/shell colloidal spheres. Adv. Mater. 19, 577–580.

Liu, Y., Martin, M., 2001. P53 protein at the hub of cellular DNA damage response pathways through sequence-specific and non-sequence-specific DNA binding. Carcinogenesis 22, 851–860.

Luo, Z., Cai, K., Hu, Y., Zhao, L., Liu, P., Duan, L., Yang, W., 2011. Mesoporous silica nanoparticles end-capped with collagen: redox-responsive nanoreservoirs for targeted drug delivery. Angew. Chem. Int. Ed. 50, 640–643.

Mamaeva, V., Sahlgren, C., Lindén, M., 2013. Mesoporous silica nanoparticles in medicine-recent advances. Adv. Drug Del. Rev. 65, 689–702.

Mossman, T., 1983. Rapid colorimetric assay for cellular growth and survival: application to proliferation and cytotoxicity assays. J. Immunol. Methods 65, 55–63.

Nakamura, Y., Tsumura, Y., Shibata, T., Ito, Y., 1997. Differences in behavior among the chlorides of seven rare earth elements administered intravenously to rats. Fundam. Appl. Toxicol. 37, 106–116.

Palasz, A., Czekaj, P., 2000. Toxicological and cytophysiological aspects of lanthanides action. Acta Biochim. Pol. 47, 1107–1114.

Pan, L., He, Q., Liu, J., Chen, Y., Ma, M., Zhang, L., Shi, J., 2012. Nuclear-targeted drug delivery of TAT peptide-conjugated monodisperse mesoporous silica nanoparticles. J. Am. Chem. Soc. 134, 5722–5725.

Patra, C.R., Moneim, S.S.A., Wang, E., Dutta, S., Patra, S., Eshed, M., Mukherjee, P., Gedanken, A., Shah, V.H., Mukhopadhyay, D., 2009. *in-vivo* toxicity studies of europium hydroxide nanorods in mice. Toxicol. Appl. Pharm. 240, 88–98.

Reeves, J.F., Davies, S.J., Dodd, N.J.F., Jha, A.N., 2008. Hydroxyl radicals (–OH) are associated with titanium dioxide (TiO_2) nanoparticle-induced cytotoxicity and oxidative DNA damage in fish cells. Mutat. Res. 640, 113–122.

Santra, S., Tapec, R., Theodoropoulou, N., Dobson, J., Hebard, A., Tan, W., 2001. Synthesis and characterization of silica-coated iron oxide nanoparticles in microemulsion: the effect of nonionic surfactants. Langmuir 17, 2900–2906.

Tang, F., Li, L., Chen, D., 2012. Mesoporous silica nanoparticles: synthesis, biocompatibility and drug delivery. Adv. Mater. 24, 1504–1534.

Taylor, K.M.L., Kim, J.S., Rieter, W.J., An, H., Lin, W., Lin, W., 2008. Mesoporous silica nanospheres as highly efficient MRI contrast agents. J. Am. Chem. Soc. 130, 2154–2155.

Upadhyaya, L., Singh, J., Agarwal, V., Tewari, R.P., 2014a. The implications of recent advances in carboxymethyl chitosan based targeted drug delivery and tissue engineering applications. J. Contr. Release 186, 54–87.

Upadhyaya, L., Singh, J., Agarwal, V., Pandey, A.C., Verma, S.P., Das, P., Tewari, R.P., 2014b. In situ grafted nanostructured ZnO/carboxymethyl cellulose nanocomposites for efficient delivery of curcumin to cancer. J. Polym. Res. 21, 1–9.

Upadhyaya, L., Singh, J., Agarwal, V., Pandey, A.C., Verma, S.P., Das, P., Tewari, R.P., 2015. Efficient water soluble nanostructured ZnO grafted O-carboxymethyl chitosan/curcumin-nanocomposite for cancer therapy. Process Biochem. 50, 678–688.

Wang, W., Sun, W., Wang, X., 2004. Intramuscular gene transfer of CGRP inhibits neointimal hyperplasia after balloon injury in the rat abdominal aorta. Am. J. Physiol. Heart Circul. Physiol. 287, H1582–H1589.

Yang, P., Quan, Z., Lu, L., Huang, S., Lin, J., 2008. Luminescence functionalization of mesoporous silica with different morphologies and applications as drug delivery systems. Biomaterials 29, 692–702.

Ye, Z., Tan, M., Wang, G., Yuan, J., 2004a. Novel fluorescent europium chelate-doped silica nanoparticles: preparation, characterization and time-resolved fluorometric application. J. Mater. Chem. 14, 851–856.

Ye, Z., Tan, M., Wang, G., Yuan, J., 2004b. Preparation, characterization, and time-resolved fluorometric application of silica-coated terbium(III) fluorescent nanoparticles. Anal. Chem. 76, 513–518.

Yu, K.O., Grabinski, C.M., Schrand, A.M., Murdock, R.C., Wang, W., Gu, B., Schlager, J.J., Hussain, S.M., 2009. Toxicity of amorphous silica nanoparticles in mouse keratinocytes. Nanopart. Occup. Health 11, 15–24.

Yu, M., Lin, J., Fang, J., 2005. Silica spheres coated with YVO_4: Eu^{3+} layers via sol-gel process: a simple method to obtain spherical core-shell phosphors. Chem. Mater. 17, 1783–1791.

Yu, S.Y., Zhang, H.J., Yu, J.B., Wang, C., Sun, L.N., Shi, W.D., 2007. Bifunctional magnetic-optical nanocomposites: grafting lanthanide complex onto core-shell magnetic silica nanoarchitecture. Langmuir 23, 7836–7840.

Zaffaroni, N., Pannati, M., Diadone, M.G., 2007. Survivin as a target for new anticancer interventions. J. Cell Mol. Med. 9, 360–372.

Zhang, Q., Liu, F., Nguyen, K.T., Ma, X., Wang, X., Xing, B., Zhao, Y., 2012. Multifunctional mesoporous silica nanoparticles for cancer-targeted and controlled drug delivery. Adv. Funct. Mater. 22, 5144–5156.

Zhao, Y., Trewyn, B.G., Slowing, I.I., Lin, V.S.Y., 2009. Mesoporous silica nanoparticle-based double drug delivery system for glucose-responsive controlled release of insulin and cyclic AMP. J. Am. Chem. Soc. 131, 8398–8400.

Zhivotosky, B., Orrenius, S., 2001. Assessment of apoptosis and necrosis by DNA fragmentation and morphological criteria. Curr. Protoc. Cell. Biol. 131 (November) (Chapter 18: Unit 18.3.0).